Author/s:
Prosser, A;Huang, WH;Liu, L;Dart, S;Watson, M;de Boer, B;Kendrew, P;Lucas, A;Larma-Cornwall, I;Gaudieri, S;Jeffrey, GP;Delriviere, L;Kallies, A;Lucas, M

Title:
Dynamic changes to tissue-resident immunity after MHC-matched and MHC-mismatched solid organ transplantation

Date:
2021-05-18

Citation:
Prosser, A., Huang, W. H., Liu, L., Dart, S., Watson, M., de Boer, B., Kendrew, P., Lucas, A., Larma-Cornwall, I., Gaudieri, S., Jeffrey, G. P., Delriviere, L., Kallies, A. & Lucas, M. (2021). Dynamic changes to tissue-resident immunity after MHC-matched and MHC-mismatched solid organ transplantation. Cell Reports, 35 (7), https://doi.org/10.1016/j.celrep.2021.109141.

Persistent Link:
https://hdl.handle.net/11343/280642

Report

Cell Reports

Dynamic changes to tissue-resident immunity after MHC-matched and MHC-mismatched solid organ transplantation

Graphical abstract

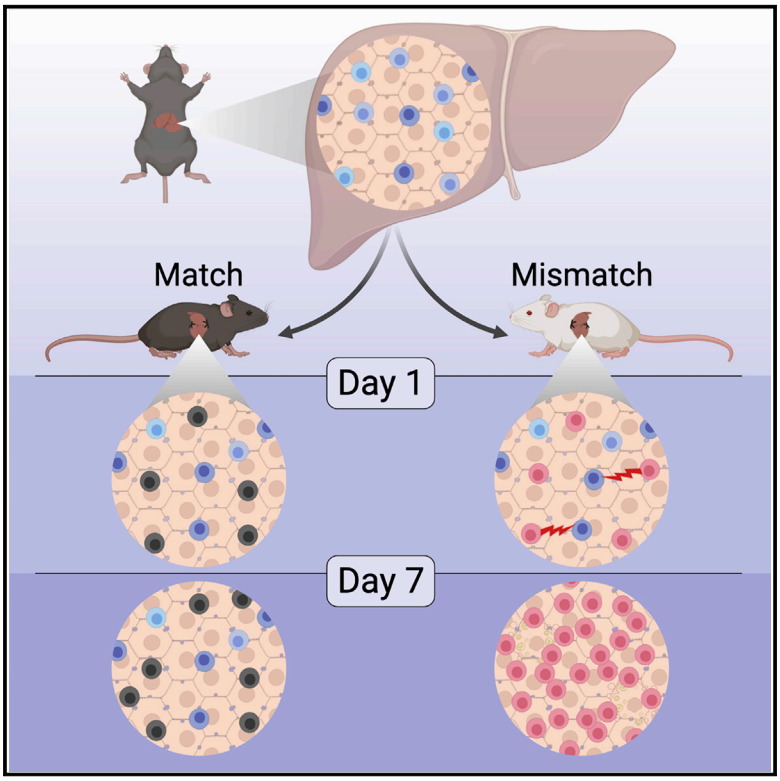

Authors

Amy Prosser, Wen Hua Huang, Liu Liu, ..., Luc Delriviere, Axel Kallies, Michaela Lucas

Correspondence

michaela.lucas@uwa.edu.au

In brief

Prosser et al. characterize tissue-resident lymphocytes in the liver and map the changes to the donor and recipient lymphocyte compartment after liver and heart transplantation in mice. The graft becomes significantly altered in comparison to a native organ, with implications for infection control and graft function.

Highlights

- The liver contains diverse, transplantable tissue-resident lymphocyte populations
- Donor lymphocytes are deleted after MHC-mismatched transplantation by recipient T and B cells
- Graft-infiltrating cells do not recreate a native organ's lymphocyte composition

Prosser et al., 2021, Cell Reports *35*, 109141
May 18, 2021
https://doi.org/10.1016/j.celrep.2021.109141

CellPress

Cell Reports

CellPress
OPEN ACCESS

Report

Dynamic changes to tissue-resident immunity after MHC-matched and MHC-mismatched solid organ transplantation

Amy Prosser,[1,2] Wen Hua Huang,[1,3] Liu Liu,[1] Sarah Dart,[1] Monalyssa Watson,[1] Bastiaan de Boer,[4] Philip Kendrew,[5] Andrew Lucas,[1] Irma Larma-Cornwall,[6] Silvana Gaudieri,[2] Gary P. Jeffrey,[1,3,7] Luc Delriviere,[1,3] Axel Kallies,[8] and Michaela Lucas[1,9,10,*]

[1]Medical School, University of Western Australia, Perth, WA 6009, Australia
[2]School of Human Sciences, University of Western Australia, Perth, WA 6009, Australia
[3]Western Australian Liver and Kidney Transplant Service, Sir Charles Gairdner Hospital, Perth, WA 6009, Australia
[4]Department of Anatomical Pathology, Pathwest Laboratory Medicine, Perth, WA 6009, Australia
[5]Department of Clinical Biochemistry, Pathwest Laboratory Medicine, Perth, WA 6009, Australia
[6]Centre for Microscopy, Characterisation and Analysis, University of Western Australia, Perth, WA 6009, Australia
[7]Department of Gastroenterology, Sir Charles Gairdner Hospital, Perth, WA 6009, Australia
[8]Department of Microbiology and Immunology, The University of Melbourne, The Peter Doherty Institute for Infection and Immunity, Melbourne, VIC 3000, Australia
[9]Department of Immunology, Sir Charles Gairdner Hospital and Pathwest Laboratory Medicine, Perth, WA 6009, Australia
[10]Lead contact
*Correspondence: michaela.lucas@uwa.edu.au
https://doi.org/10.1016/j.celrep.2021.109141

SUMMARY

The heterogeneous pool of tissue-resident lymphocytes in solid organs mediates infection responses and supports tissue integrity and repair. Their vital functions in normal physiology suggest an important role in solid organ transplantation; however, their detailed examination in this context has not been performed. Here, we report the fate of multiple lymphocyte subsets, including T, B, and innate lymphoid cells, after murine liver and heart transplantation. In major histocompatibility complex (MHC)-matched transplantation, donor lymphocytes are retained in liver grafts and peripheral lymphoid organs of heart and liver transplant recipients. In MHC-mismatched transplantation, increased infiltration of the graft by recipient cells and depletion of donor lymphocytes occur, which can be prevented by removal of recipient T and B cells. Recipient lymphocytes fail to recreate the native organs' phenotypically diverse tissue-resident lymphocyte composition, even in MHC-matched models. These post-transplant changes may leave grafts vulnerable to infection and impair long-term graft function.

INTRODUCTION

Transplantation of a functioning solid organ from one individual to another remains one of the greatest modern medical advancements and is the final treatment option for end-stage organ failure. Despite significant advances in the prevention of acute rejection of transplanted organs, 30%–70% of liver, kidney, heart, and lung transplants fail within 10 years (ANZCOTR, 2018; ANZDATARegistry, 2018; ANZLITR, 2020; OPTN/SRTR, 2020). Contributors to graft failure include ongoing chronic rejection, impaired infection control, and immunosuppressant drug toxicities, highlighting the significant clinical need for improved understanding in this field.

It has long been appreciated that organ transplantation involves the simultaneous transfer of immune cells, historically termed donor passenger leukocytes, which were originally presumed to be of myeloid origin (Elkins and Guttmann, 1968). More recently, tissue-resident lymphocytes (TRLs) have been described that do not recirculate in the blood or lymphatics and occupy nonlymphoid tissues (Fan and Rudensky, 2016; Steinert et al., 2015). Retention of TRLs in tissue is achieved by repression of egress through downregulation of cell migration molecules such as S1PR1, CCR7, and CD62L and promotion of active retention through binding of receptors and integrins, including CD69, CD49a, and CD103, to extracellular matrix components (Mackay and Kallies, 2017; Mackay et al., 2016).

TRLs reside predominantly at sites of previous infection and common pathogen entry (Belz et al., 2020). Here, they orchestrate the control of invading pathogens via rapid production of cytokines and instigation of cellular recruitment to infected tissue (Ariotti et al., 2014; Fan and Rudensky, 2016). TRLs also contribute to repair of damaged tissue, cancer surveillance, and homeostasis by production of growth factors and immunomodulatory cytokines (Gebhardt et al., 2018; Klose and Artis, 2016). Damaged tissue repair is an inevitable requirement after transplantation surgery, and the protective functions of TRLs

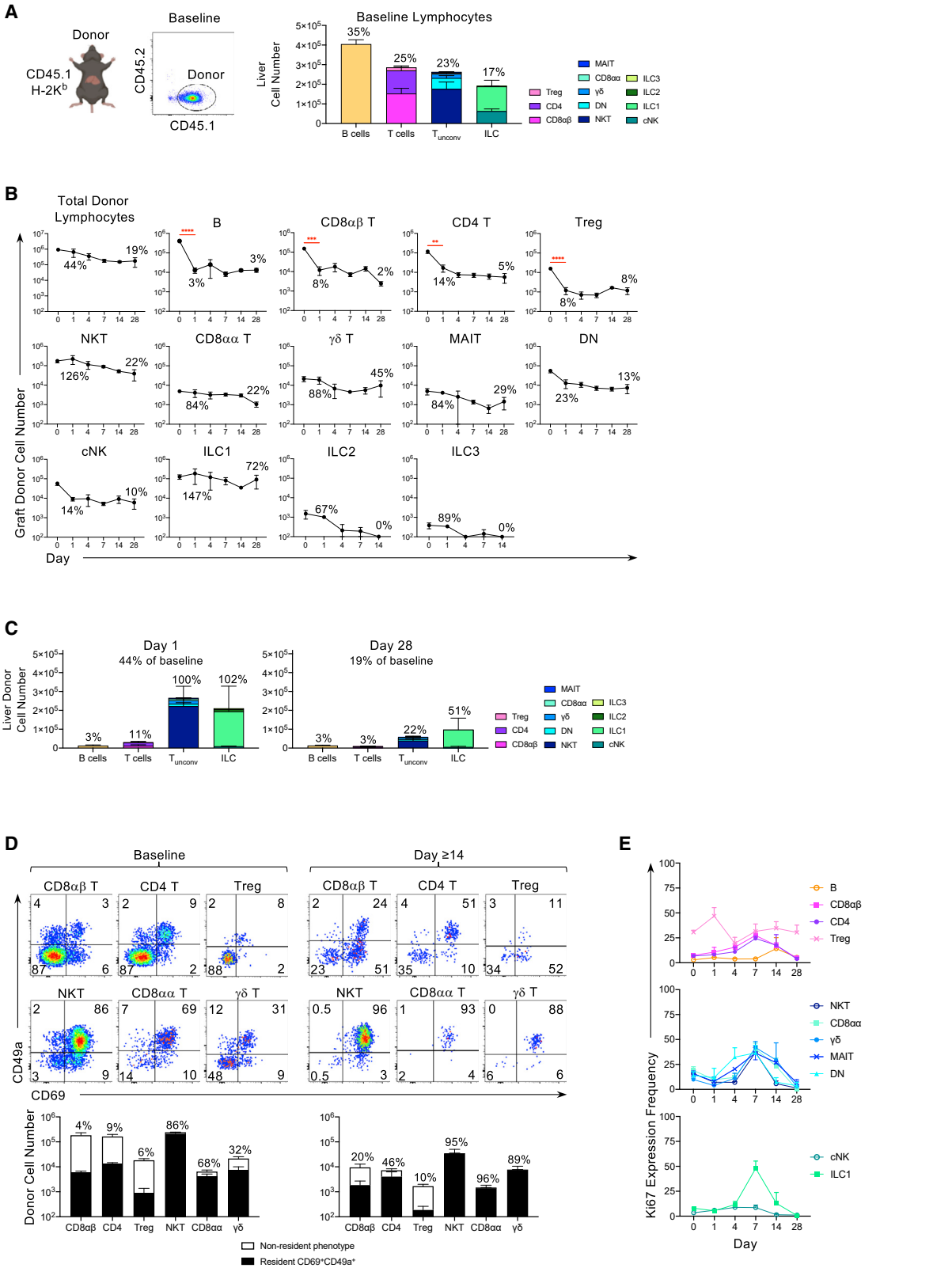

(legend on next page)

may contribute to the resolution of infections and latent viral reactivation, both of which are common post-transplant complications (Prosser et al., 2018; Sen et al., 2019).

The persistence of donor-derived CD8 and CD4 T cells has been described within grafts after liver, lung, and kidney transplantation in humans (de Leur et al., 2019; Pallett et al., 2020; Snyder et al., 2019). However, because of the difficulties in obtaining human graft tissue, detailed analysis of other TRL subsets has not been performed. Human studies are confounded by the genetic and clinical heterogeneity of study subjects and the treatment of patients with divergent systemic immunosuppressive regimes. TRL biology has predominantly been studied using murine parabiosis experiments but rarely in rodent models of transplantation, primarily because of their high level of technical difficulty. So far, only one study of murine orthotopic liver transplantation has described the limited retention of donor lymphocytes 48 h after transplantation, without studying tissue residency in detail (Tay et al., 2013). Murine models of solid organ transplantation offer the advantages of controlled genetic heterogeneity without tissue sampling limitations, underscoring their suitability to increase our knowledge of TRL biology that has been gathered from human transplantation and parabiosis approaches.

Here, we have examined 13 lymphocyte subsets before and after major histocompatibility complex (MHC)-matched and MHC-mismatched murine liver and heart transplantation. These subsets include conventional T (CD8$\alpha\beta$ and CD4) cells and regulatory T (Treg) cells; B cells; unconventional T cells, including natural killer T (NKT) cells, mucosal-associated invariant T (MAIT) cells, $\gamma\delta$ T cells, CD8$\alpha^+\beta^-$ (CD8$\alpha\alpha$) T cells, and TCRβ^+ CD4$^-$CD8$^-$ double-negative (DN) T cells; and innate lymphoid cells (ILCs), including conventional natural killer (cNK), ILC1, ILC2, and ILC3 populations. After MHC-matched transplantation, phenotypically heterogeneous donor TRLs were retained in the liver graft while recirculating donor lymphocytes were found in the peripheral lymphoid organs of liver and heart transplant-recipient mice. In contrast, complete MHC-mismatched transplantation led to donor lymphocyte deletion and greater recipient infiltration to both liver and heart grafts. In a model of nonpharmacological immunosuppression using T cell- and B cell-deficient recombinase activating gene 1 knockout (*Rag1*$^{-/-}$) mice as recipients, donor lymphocytes were retained in both MHC-matched and MHC-mismatched liver transplants. Liver and heart graft organs developed persistent changes in their lymphocyte numbers, composition, and phenotype compared with baseline organs. Overall, these data provide insights into the dynamics of tissue-resident immunity fluctuations after solid organ transplantation with or without MHC mismatch and the impact that recipient immune pressure has on these changes.

RESULTS

Liver TRLs are retained and proliferate after transplantation

We analyzed the fate of liver TRLs after MHC-matched liver transplantation using congenically matched mouse strains for distinction between donor (CD45.1) and recipient (CD45.2) leukocytes. Pretransplant baseline livers from CD45.1 mice were flushed before processing to replicate the transplantation procedure and to remove most circulating lymphocytes. On average, 10^6 lymphocytes were detected per liver, most of which were B cells, followed by similar proportions of conventional and unconventional T cells and a smaller population of ILCs (Figures 1A, S1A, and S1B). After MHC-matched transplantation, 56% of total donor lymphocytes, including >85% of donor B, conventional T, and cNK cells, were lost from the graft within one day, whereas <16% of donor unconventional T cells and ILC1 had exited the graft at the same time point (Figures 1B and 1C). Donor ILC2 and ILC3 were undetectable by day 14 and were not investigated further (Figure 1B). Although only 19% of the baseline number of donor lymphocytes were retained at day 28, unconventional T cells and ILC1 became the predominant subsets (Figures 1B and 1C).

The canonical markers of T cell tissue residency, CD69 and CD49a, were measured on donor T cells at baseline and those retained in the liver graft for $\geq$14 days after transplantation (Figure 1D). At baseline, the liver contained heterogeneous populations of all T cells, with most conventional T cells expressing neither CD69 nor CD49a. Combined with the observed loss of most these cells from the graft within one day, this indicates that they were not resident but likely recirculating cells. Donor T cell subsets that were retained in the liver graft for $\geq$14 days were enriched for a CD69$^+$CD49a$^+$ phenotype, although conventional T cells retained significant heterogeneity. In contrast, NKT and CD8$\alpha\alpha$ T cells retained their predominantly CD69$^+$CD49a$^+$ phenotype from baseline to $\geq$14 days after transplantation.

Extensive proliferation of most donor lymphocyte populations occurred after transplantation, indicating their potential to self-renew (Figure 1E). Compared with other populations, Treg cells were the most proliferative before and immediately after transplantation, peaking at day one post-transplant. Thus, although most donor conventional lymphocyte subsets were rapidly lost from the transplanted liver, a small proportion of these cells, along with most unconventional T cells and ILC1, were retained and proliferated in the graft.

Figure 1. Donor lymphocytes are retained and proliferate after MHC-matched liver transplantation and do not all express a canonical tissue-resident phenotype

(A) Baseline liver lymphocytes (n = 5–10). Percentages are means of total lymphocytes.

(B) Donor lymphocyte numbers in the liver after transplantation (n = 2–10, unpaired t test and Mann-Whitney test). Percentages are means of baseline numbers at days 1 and 28.

(C) Liver graft donor lymphocyte composition (n = 3–7). Percentages are means of baseline numbers.

(D) Donor T cell expression of CD69 and CD49a at baseline (n = 5–10) and day $\geq$14 (n = 4–6). Bar graphs show means of donor cell numbers expressing a CD69$^+$CD49a$^+$ phenotype (black bars) or not (white bars). Percentages are mean expression frequencies of a CD69$^+$CD49a$^+$ phenotype.

(E) Donor lymphocyte Ki67 expression (n = 2–10).

Data are means with SEM. Symbols indicate: **p < 0.01; ***p < 0.001; ****p < 0.0001. See also Figures S1 and S3.

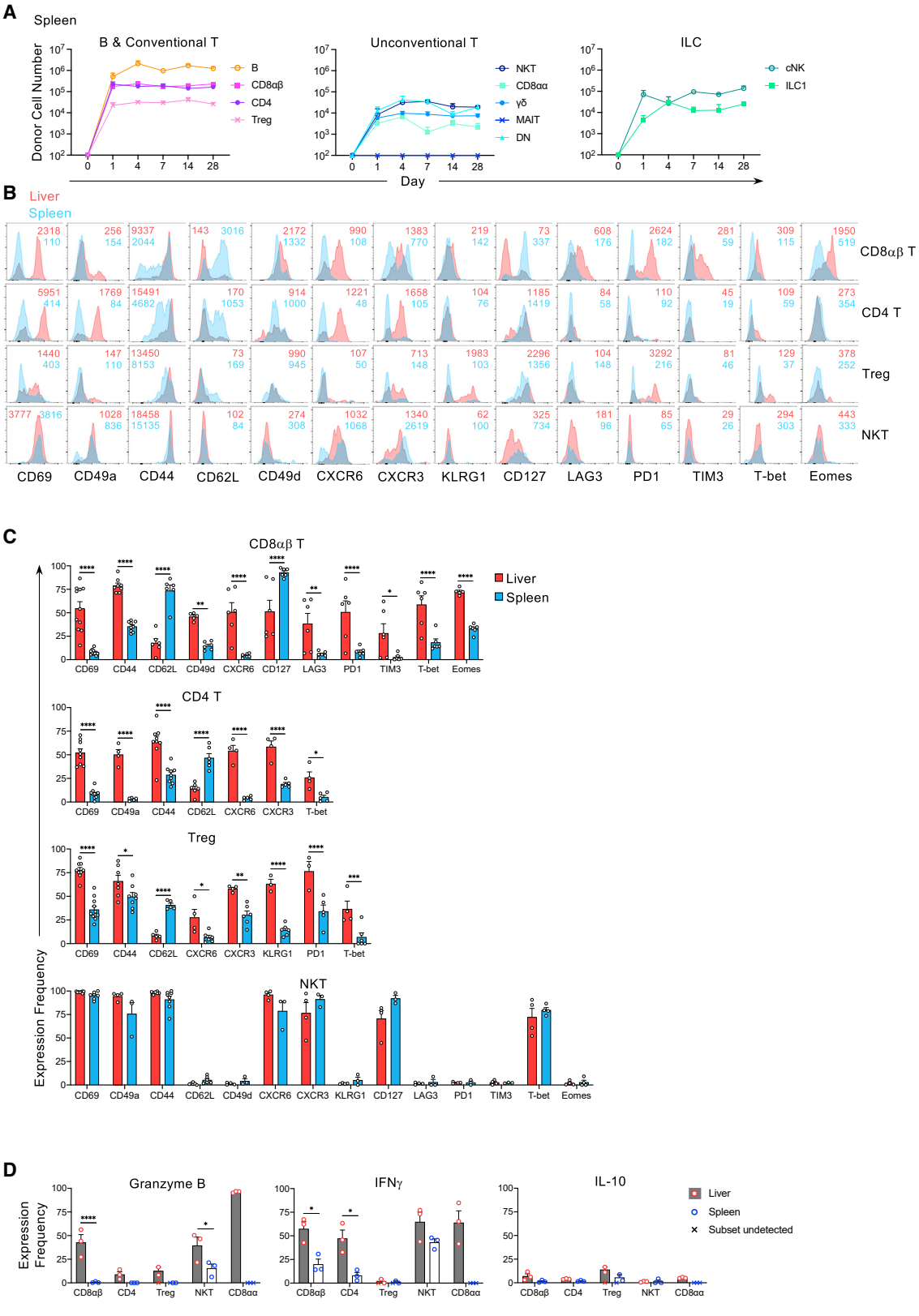

(legend on next page)

Donor lymphocytes that exit the liver persist in the periphery but differ from TRLs

After MHC-matched liver transplantation, donor lymphocytes were detected in the spleen, lymph nodes (LNs), bone marrow (BM), and blood, with greatest numbers found in the spleen (Figures 2A and S2A). Generally, B cells and conventional T cells persisted in the periphery at higher numbers than unconventional T cells and ILC1. Preservation of the total donor lymphocyte pool transplanted with the liver was assessed by summation of donor cell numbers from the liver graft, spleen, LNs, BM, and blood at day 28 post-transplant (Figure S2B). At day 28, donor lymphocyte numbers had increased by >2-fold, driven by expansion of B, CD8$\alpha\beta$ T, CD4 T, Treg, and cNK cells. These subsets proliferated predominantly in the liver graft, and at later time points, B and Treg cells proliferated in the LNs (Figures 1E and S2C).

The phenotype of donor tissue-resident T cells retained in the liver for $\geq$14 days was then compared with donor cells in the spleen (Figures 2B and 2C). Markers of T cell memory, chemokine receptors, activation, co-inhibition, and transcription factors were assessed. CD8$\alpha\beta$ T, CD4 T, and Treg cells were examined as the T cell subsets with the largest egress to the periphery and contrasted to NKT cells, which were mostly retained in the liver. Across the subsets, expression of CD69, CD44, CXCR6, and T-bet was enriched in graft-resident compared with splenic donor conventional T cells, whereas CD62L was increased on splenic cells. Liver-resident CD8$\alpha\beta$ T cells also had increased expression of the inhibitory receptors LAG3, PD1, and TIM3 compared with their splenic counterparts, with PD1 expression also increased on tissue-resident Treg cells. Graft-resident and splenic donor NKT cells did not differ in phenotype.

Donor graft-resident and splenic T cells were further characterized by measurement of their functional capacity at day 7 (Figures 2D and S2D). Granzyme B and interferon γ (IFNγ) production was increased in liver-resident cells, with 40% of graft-resident CD8$\alpha\beta$ T and NKT cells expressing granzyme B compared with 0%–15% in the spleen (Figure 2D). All resident CD8$\alpha\alpha$ T cells produced granzyme B, with most co-expressing IFNγ. IFNγ was also expressed by more liver-resident than splenic donor CD8$\alpha\beta$ and CD4 T cells. Interleukin-10 (IL-10) expression was low for all donor subsets, and donor Treg cells in both the liver and the spleen produced little granzyme B, IFNγ, or IL-10. These data highlight the significant phenotypic and functional differences between donor T cells resident in the liver graft and those that recirculated to the periphery after transplantation.

Recipient lymphocytes rapidly infiltrate the liver graft and differ from donor TRLs

Recipient lymphocytes entered the graft within one day of MHC-matched liver transplantation, dominating most subsets after transplantation (Figure 3A). After this initial influx, further accumulation of recipient cells did not occur. The abundant population of recipient lymphocytes at day 28 post-transplant were predominantly B cells and conventional T cells, with limited numbers of unconventional T cells and ILCs (Figure 3B).

At day 28, most graft-infiltrating recipient T cells robustly expressed CD69, with substantial co-expression of CD49a by NKT and CD8$\alpha\alpha$ T cells, similar to their donor counterparts (Figures 1D and 3C). A small proportion, yet translating to substantial numbers, of CD8$\alpha\beta$ and CD4 T cells were also CD69$^+$CD49a$^+$ (Figure 3C). No recipient Treg cells were CD69$^+$CD49a$^+$, and recipient, unlike donor, $\gamma\delta$ T cells were predominantly CD69$^-$CD49a$^-$ (Figures 1D and 3C). Further phenotypic analysis revealed recipient CD8$\alpha\beta$ T and NKT cells were most similar to their tissue-resident donor counterparts, whereas CD8$\alpha\alpha$ and CD4 T cells were most dissimilar to donor cells, particularly in expression of memory markers and chemokine receptors (Figure 3D).

Donor and recipient T cells also exhibited some differences in functional capacity by expression of granzyme B, IFNγ, and IL-10 (Figure 3E). Donor CD8$\alpha\beta$ and CD8$\alpha\alpha$ T cells expressed more granzyme B than recipient cells, whereas IFNγ expression was similar among all donor and recipient T cell subsets. IL-10 was not significantly expressed by any subset tested from either donor or recipient. Altogether, these data show that some populations of recipient cells infiltrating MHC-matched liver grafts acquire a tissue-resident phenotypic and functional profile, whereas others remain distinctly different.

The preponderance of recipient cells in the graft resulted in a significantly altered lymphocyte pool compared with a baseline liver. Combined donor and recipient cell data revealed a 1.95-fold increase in total lymphocyte number and altered subset composition, predominantly because of B cell and CD8$\alpha\beta$ T cell infiltration (Figures S3A–S3C). The overall phenotype of T cells in the day 28 graft showed an increase in expression of memory and exhaustion markers and of chemokine receptors compared with baseline (Figure S3D). Thus, transplantation even in MHC-matched settings substantially alters liver lymphocyte number, composition, and phenotype.

Cardiac lymphocyte composition is altered after MHC-matched transplantation

We next studied alterations to the cardiac lymphocyte pool after heterotopic heart transplantation. Despite being a lymphocyte-poor organ compared with the liver, all subsets were detected in the baseline heart (Figure 4A). B cells formed most of the lymphocyte pool, with substantial numbers of CD8$\alpha\beta$ and CD4 T cells and low numbers of Treg cells, unconventional T cells, and ILCs. Similar to the liver model, MHC-matched transplantation led to the loss of significant numbers of donor lymphocytes

Figure 2. Non-resident donor lymphocytes egress to and are maintained in the periphery, express a distinct phenotype, and have limited functional capacity after MHC-matched liver transplantation

(A) Splenic donor lymphocyte numbers (n = 2–9).

(B) Representative histograms of donor T cell phenotypes at day 28. Median fluorescence intensity (MFI) is indicated.

(C) Marker expression frequency by donor T cells at day $\geq$14 (n = 3–10).

(D) Donor T cell expression of granzyme B, IFNγ, and IL-10 by donor T cells at day 7 (n = 3). x indicates insufficient cell numbers for analysis.

Data are means with SEM, and 2-way ANOVA was performed. Symbols indicate: *p < 0.05; **p < 0.01; ***p < 0.001; ****p < 0.0001. See also Figure S2.

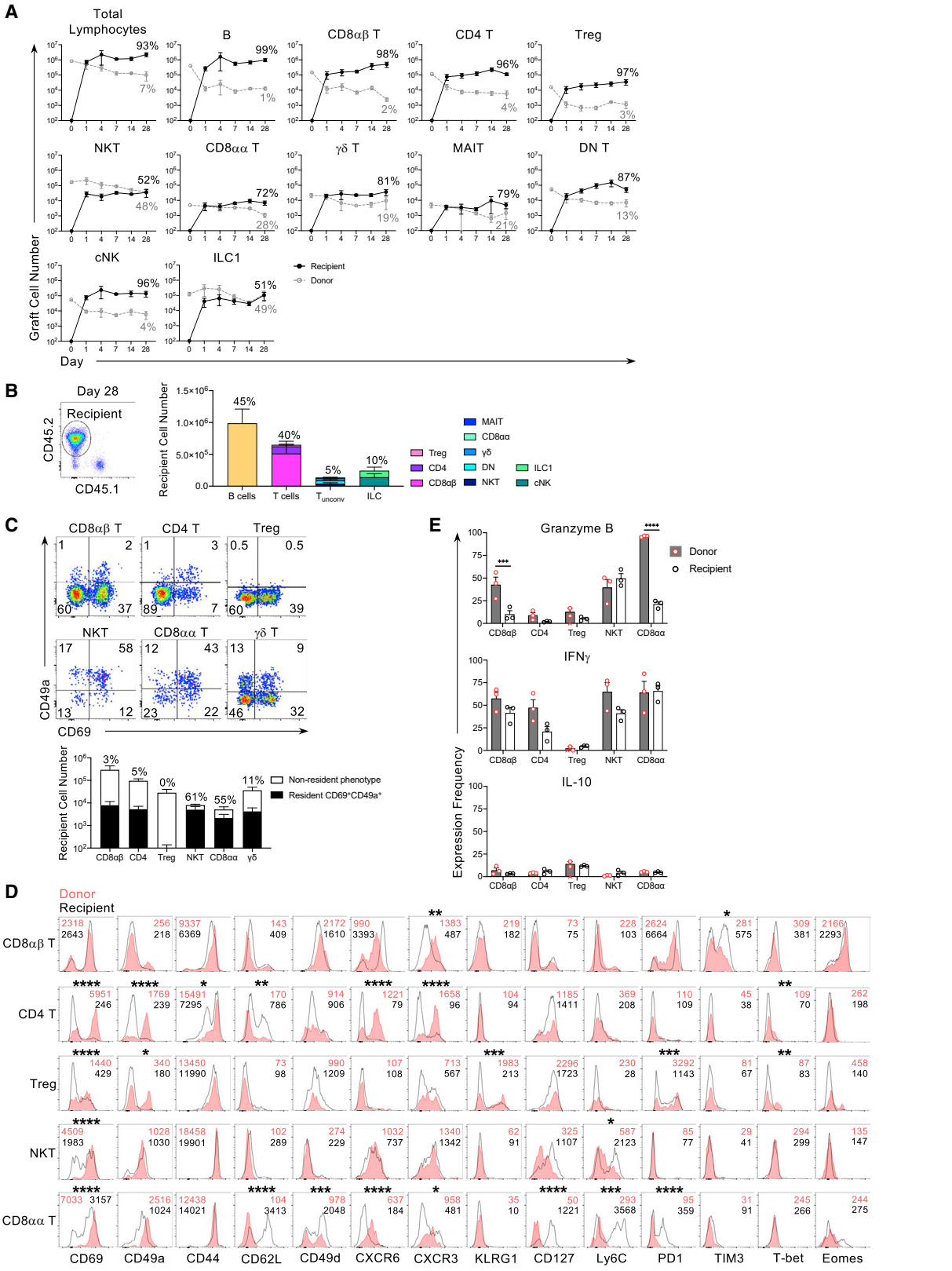

(legend on next page)

from the heart within one day of transplantation, specifically B cells, conventional T cells, and DN T cells (Figure 4B). By day 28 post-transplant, 99% of donor lymphocytes had exited the graft, indicating the lymphocyte pool detected at baseline consisted primarily of nonresident cells (Figures 4B and 4C). Minimal numbers ($<10^3$) of donor B cells, conventional T cells, DN T cells, and ILC1 were retained in the heart graft long term. Peripheral donor B cells, conventional T cells, and cNK cells were detected in the spleen; B cells and conventional T cells were detected in the LNs; and B cells only were detected in the BM (Figure S4). Infiltration of recipient lymphocytes to the heart occurred within one day of transplantation, with recipient conventional T, NKT, and CD8$\alpha\alpha$ T cells continuing to accumulate over time, leading to a >3-fold increase in total heart lymphocytes and an altered composition of lymphocytes by day 28 (Figures 4B and 4D).

Because of the small number of lymphocytes in the heart, phenotypic analysis of T cells was restricted to CD69, CD44, and CD62L (Figures 4E and 4F). Compared with baseline, the combined donor and recipient conventional T cell populations had increased CD69 and decreased CD62L expression after transplantation. Overall, the changes to the cardiac graft and periphery of the recipient after transplantation followed dynamics similar to those of the transplanted liver but also revealed organ-specific differences.

Donor lymphocytes are depleted by recipient cells after MHC-mismatched transplantation

We next assessed the fate of lymphocytes in complete MHC-mismatched liver and heart transplants without pharmacological immunosuppression. Mismatched liver grafts underwent a process of acute rejection followed by graft tolerance, with lobule inflammation and endothelialitis observed at day 7 but resolving by day 28 (Figures 5A and 5B). This is consistent with the previously described maintenance of murine liver transplants, irrespective of MHC mismatches (Qian et al., 1994). In contrast to our MHC-matched data, all donor lymphocytes were progressively depleted within one month after transplantation (Figure 5C). Depletion of peripheral donor lymphocytes also occurred after they were detected at day 1 and, for B and cNK cells, day 7, but not at day 28 post-transplant (Figure S5A).

Substantial numbers of recipient lymphocytes rapidly infiltrated the mismatched liver to a greater extent than in the MHC-matched model (10-fold more at day 7 and 3-fold more at day 28), which was driven by conventional T cells (Figures 5C and S5B). Recipient T cells were assessed for expression of granzyme B, IFNγ, and IL-10 to identify the functional capacity of these cells and whether they were likely responsible for the observed donor lymphocyte depletion (Figure 5D). In mismatched grafts, >85% of all T cell subsets expressed granzyme B, with these CD8$\alpha\beta$ T, CD4 T, and Treg cells also expressing IL-10, both at greater frequencies than in matched grafts. However, IFNγ was expressed by few T cells in mismatched grafts but by nearly half of the recipient CD8$\alpha\beta$ T, NKT, and CD8$\alpha\alpha$ T cells in matched grafts.

To study the consequences of effective suppression of recipient T and B cells on donor lymphocyte fate, we performed liver transplants into T cell- and B cell-deficient mice that are *Rag1*$^{-/-}$ recipients (Figures 5E and S5C). MHC-mismatched transplantation into *Rag1*$^{-/-}$ recipients resulted in retention of all donor lymphocyte subsets at day 7, in contrast to the substantial losses observed after immunocompetent mismatched transplants (Figures 5C and 5E). This indicates that removal or functional suppression of recipient T and B cells is sufficient to preserve donor lymphocytes in a mismatched context. When we performed MHC-matched transplants into *Rag1*$^{-/-}$ recipients, all donor lymphocyte subsets were retained at numbers similar to baseline, albeit with a loss of B cells, as observed after immunocompetent transplantation (Figure S5C). These data suggest that recipient T and B cells affect the displacement and survival of donor lymphocytes and dictate significant changes to the liver lymphocyte composition after MHC-matched and MHC-mismatched transplantation.

In contrast to the liver transplant model, the MHC-mismatched heart transplantation model does not result in long-term graft tolerance without immunosuppression (Figure 5F). Mismatched graft failure occurred by day 12 post-transplant, whereas syngeneic and congenic heart transplants survived for up to 100 days. As seen in MHC-matched hearts, donor lymphocytes were progressively lost from mismatched hearts (Figure 5G). Donor lymphocytes were also depleted from the periphery, although some donor B cells persisted in the spleen and LNs and $\gamma\delta$ T cells persisted in the BM (Figure S5D). There was a large influx of recipient lymphocytes, with greater numbers infiltrating MHC-mismatched than MHC-matched heart grafts (43-fold at day 1 and 213-fold at day 7) (Figure S5E). In summary, donor lymphocytes were rapidly depleted and replaced by an increasing number of cytotoxic recipient lymphocytes in MHC-mismatched liver and heart transplants.

DISCUSSION

The importance of tissue-resident immunity in maintaining organ physiology and defense against pathogens and cancer is becoming increasingly recognized; however, its role in the context of solid organ transplantation is less well understood. Here, we have investigated the destiny of TRL subsets in MHC-matched and MHC-mismatched murine liver and heart transplantation.

Figure 3. MHC-matched liver grafts are rapidly infiltrated by recipient lymphocytes that are distinct from donor TRLs

(A) Donor and recipient lymphocyte numbers (n = 2–9). Percentages are means of recipient and donor contributions to each subset at day 28.

(B) Graft-infiltrating recipient lymphocytes at day 28 (n = 3–7). Percentages are means of total recipient lymphocytes.

(C) Recipient T cell expression of CD69 and CD49a at day 28 (n = 4–6). Bar graphs show means of recipient cell numbers expressing a CD69$^+$CD49a$^+$ phenotype (black bars) or not (white bars). Percentages are mean expression frequencies of a CD69$^+$CD49a$^+$ phenotype.

(D) Representative histograms of T cell phenotypes at day 28 (n = 3–12, 2-way ANOVA on expression frequency data). MFI is indicated.

(E) Recipient T cell granzyme B, IFNγ, and IL-10 expression at day 7 (n = 3, 2-way ANOVA). x indicates insufficient cell numbers for analysis.

Data are means with SEM. Symbols indicate: *p < 0.05; **p < 0.01; ***p < 0.001; ****p < 0.0001. See also Figure S3.

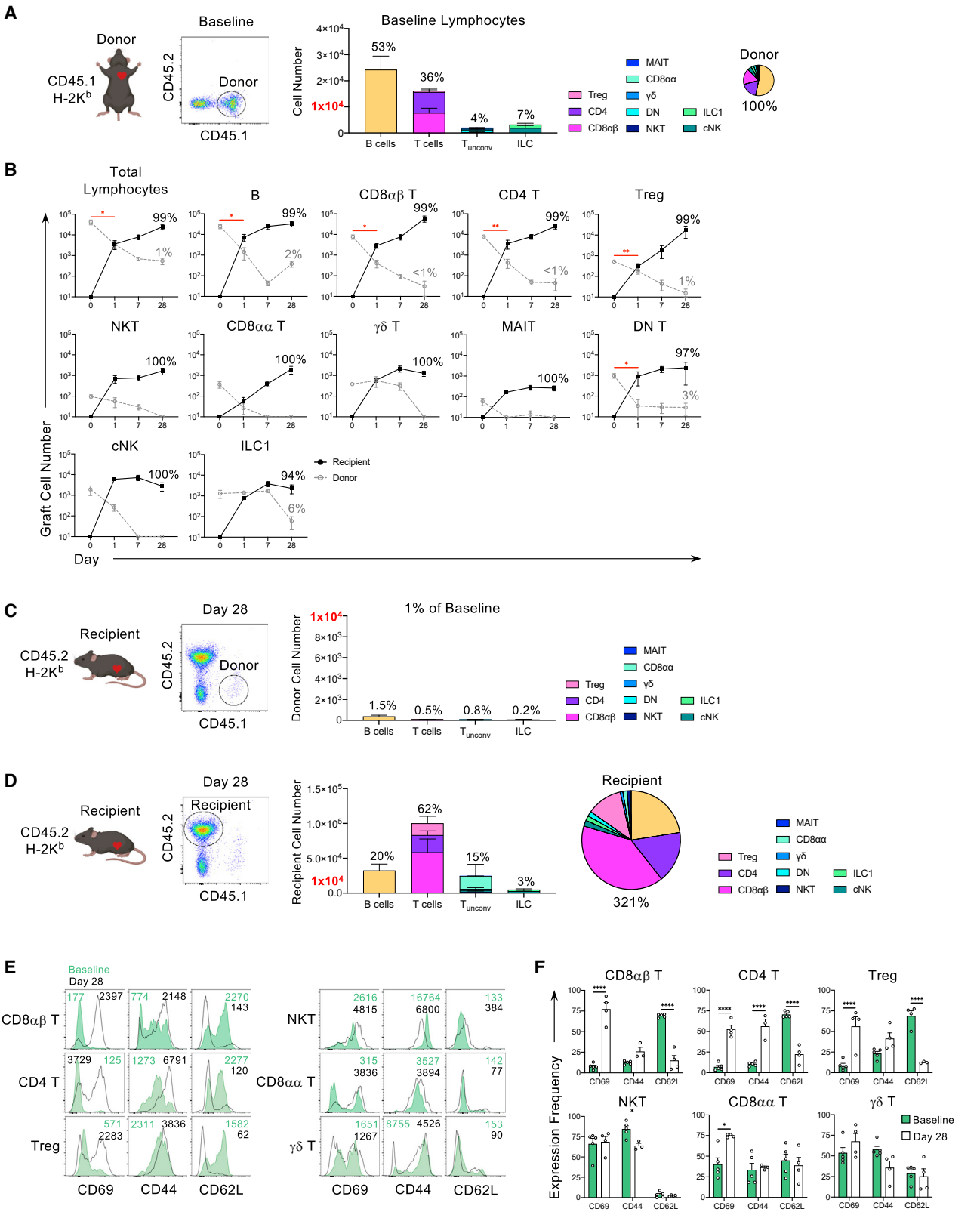

(legend on next page)

We have identified and characterized long-term tissue-resident populations of B cells, conventional and unconventional T cells, and ILCs that are maintained after liver transplantation. This confirms previous parabiosis and infection studies that have described tissue-resident CD8 T cells (Steinert et al., 2015), CD4 T cells (Beura et al., 2019), NKT cells (Geissmann et al., 2005), γδ T cells (Li et al., 2017), MAIT cells (Salou et al., 2019), and ILC1 (Gasteiger et al., 2015) in the murine liver. CD8 and CD4 T cells have also recently been shown to persist in human liver transplants in patients on iatrogenic immunosuppression (Pallett et al., 2020). Outside of the liver, resident memory B cells have been described in the murine lung and spleen and tissue-resident Treg cells have been described in the visceral adipose tissue and intestine (Allie et al., 2019; Feuerer et al., 2009; Johnson et al., 2020; Makita et al., 2007). TCRβ$^+$ DN and CD8αα T cells, which we carefully analyzed to ensure they were not γδ T, MAIT, or NKT cells, are abundant populations in the liver but have not previously been assessed for tissue residency (Hossain et al., 2000; Norris et al., 1998).

We found that CD8αα T cells can comprise up to 11% of CD8 T cells in the liver. These cells are not MHC class I restricted and have been described alternately as self-reactive regulatory T cells or hyperfunctional effector T cells in various models (Cheroutre and Lambolez, 2008; Poussier et al., 2002; Vinton et al., 2017). In our MHC-matched liver transplants, CD8αα T and NKT cells were the closest to classical tissue-resident T cells because of their long-term retention and homogeneous, canonical phenotype. CD8αα T cells also highly expressed granzyme B, indicative of front-line cytotoxicity. Several studies have reported on tissue-resident CD8 T cells in the liver, although none have distinguished between the markedly different subsets of CD8αα and CD8αβ (Fernandez-Ruiz et al., 2016; Holz et al., 2018; Mackay et al., 2016; Steinert et al., 2015).

Analysis of TRLs after MHC-matched liver transplantation revealed significant heterogeneity in the expression of canonical tissue-resident markers. Recent reports have also highlighted phenotypic diversity of tissue-resident CD8 T cells in other models (Milner et al., 2020). Expression of CD69 and CD49a, originally thought to be defining markers of tissue residency, has been shown to be variable, tissue dependent, and dispensable for tissue-resident CD8 T cells (Haddadi et al., 2017; Topham and Reilly, 2018; Walsh et al., 2019). However, our observed phenotypic diversity may be explained by the post-transplant pool of donor conventional T cells consisting of a combination of graft-resident cells and recirculating cells trafficking to and from the graft. Our donor unconventional T cell populations, which exhibited limited egress from the transplanted liver and homogeneously expressed markers of tissue residency, support this explanation. Furthermore, because we observed self-renewal of graft-resident populations, some of these donor cells may not have gained expression of expected tissue-resident markers at the point of our analysis.

Additional markers were examined to determine their greater suitability than CD69 and CD49a in defining tissue-resident populations in the transplanted liver. Interactions of CXCR6 with CXCL16 in liver sinusoids (Heesch et al., 2014), CXCR3 with CXCL10 in hepatic lobules after ischemia and reperfusion (Zhai et al., 2008), and PD1 with hepatocyte PD-L1 have been shown to enhance tissue residency in the liver (Gill et al., 2019; Pallett et al., 2017). Persistent low-level expression of T-bet and downregulation of Eomes controls tissue-resident CD8 T cell formation in the skin and lungs (Mackay et al., 2015). In our liver grafts, donor conventional T cells were enriched but remained heterogeneous for CXCR6, CXCR3, and PD1 expression. Despite the expression of PD1, TIM3, and LAG3, graft-resident T cells retained expression of granzyme B and IFNγ. These inhibitory molecules on tissue-resident T cells in the context of transplantation therefore appear to be associated with checkpoint inhibition and/or tissue retention rather than exhaustion. Although low-level T-bet expression was observed in our graft-resident donor and infiltrating recipient T cells, Eomes was not downregulated, suggesting different transcriptional requirements for liver than skin or lung tissue residency. The heterogeneity we observed in TRLs retained in liver grafts provides intriguing insights into the subset-, location-, and context-dependent phenotype of these cells.

Comparison of MHC-matched and MHC-mismatched liver transplantation revealed striking differences in donor and recipient lymphocyte responses. Mismatched liver grafts underwent a transient rejection episode that peaked at day 7 and in most cases was overcome and resolved within one month without pharmacological immunosuppression. This is consistent with human findings in which acute T cell-mediated rejection is common in the first 6 weeks after transplantation; nevertheless, 20%–60% of liver transplant recipients can achieve tolerance for >1 year after withdrawal of immunosuppression therapy (Feng and Bucuvalas, 2017; Taner, 2017). In our study, all donor lymphocytes were depleted from the MHC-mismatched liver graft and periphery by day 28 post-transplant, and most were depleted by day 7. This depletion most likely results from the cytotoxic effect of recipient T cells, as suggested by their near-ubiquitous expression of granzyme B. In contrast to the chimerism observed in our MHC-matched model, the deletion of donor lymphocytes after MHC-mismatched transplantation meant neither graft nor peripheral chimerism was achieved and was not necessary for tolerance. However, it cannot be excluded

Figure 4. The murine heart does not retain donor lymphocytes after MHC-matched transplantation but is rapidly infiltrated by recipient cells that alter the cardiac lymphocyte pool

(A) Baseline heart lymphocytes (n = 5). Percentages are means of total lymphocytes.

(B) Donor and recipient lymphocyte numbers (n = 3–5, unpaired t tests between baseline and donor cells at day 1). Percentages are mean donor and recipient contributions to each subset at day 28.

(C and D) Heart graft donor (C) and recipient (D) lymphocytes at day 28 (n = 3–4). Percentages are means of baseline or total recipient lymphocytes, respectively.

(E) Representative histograms of combined donor and recipient T cell phenotypes (n = 3–5). MFI is indicated.

(F) Donor plus recipient T cell marker expression frequency (n = 3–5, 2-way ANOVA).

Data are means with SEM. Symbols indicate: *p < 0.05; **p < 0.01; ****p < 0.0001. See also Figure S4.

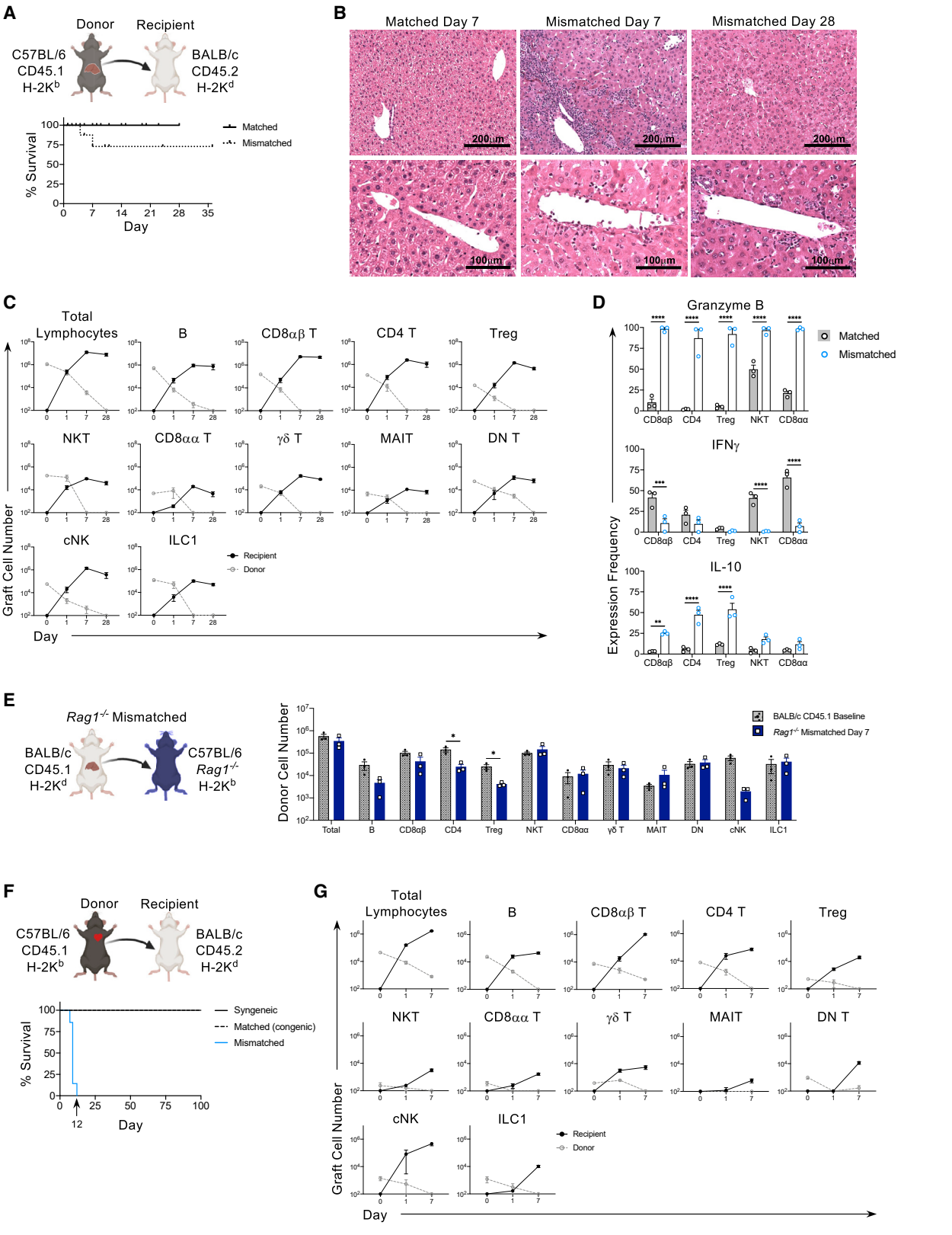

(legend on next page)

that the transient presence of donor lymphocytes before their depletion contributed to the induction of liver acceptance.

Donor lymphocyte loss from both MHC-matched and MHC-mismatched liver grafts was prevented by transplantation into *Rag1*$^{-/-}$ recipient mice, confirming the role of recipient T and B cells in donor cell depletion. The retention of donor lymphocytes in this *Rag1*$^{-/-}$ model of effective T and B cell suppression aligns with findings after human liver transplantation of donor lymphocyte persistence over several years (Pallett et al., 2020). The maintenance observed in humans is likely a product of the long-term immunosuppression used to suppress rejection responses. Snyder et al. (2019) have reported that human lung transplant recipients with higher frequencies of donor T cells in their bronchoalveolar lavage fluid experienced fewer adverse clinical events, including fewer rejection episodes. What remained unclear is whether the retention of donor lymphocytes resulted in fewer rejection episodes or whether greater numbers of donor lymphocytes were retained because of fewer or less severe rejection episodes. Our MHC-mismatched data indicate that the rejection episodes determine the number of retained donor lymphocytes after transplantation. One can further speculate that the type of immunosuppression used in humans differentially influences specific donor lymphocyte subsets after transplantation.

Finally, we have compared our findings in the liver to a heart transplantation model in which rejection occurs of MHC-mismatched grafts. The heart is a lymphocyte-poor organ, with 22-fold fewer total lymphocytes than the liver at baseline, which proved to be primarily transient, nonresident cells, as indicated by their near-complete loss from both MHC-matched and MHC-mismatched grafts. Significant infiltration of heart grafts occurred, resulting in drastically altered lymphocyte compositions and ultimately the failure of mismatched hearts. Altogether, these data show that without immunosuppression of the recipient, donor lymphocytes are not maintained after MHC-mismatched solid organ transplantation. Donor immunological memory and direct recognition of donor MHC-presented antigen are lost, leaving the graft vulnerable to infection and with potentially impaired physiological function.

Our two models of solid organ transplantation have provided insights into the fate of circulating and tissue-resident donor lymphocytes. Tissue-resident immunity is disturbed after transplantation, which is likely to contribute to post-transplant infections, cancer, and poor long-term graft outcomes by affecting normal physiological and immune functions. Significant infiltration of recipient lymphocytes to both liver and heart grafts occurred, although the native organs' phenotypically and functionally diverse TRL composition was not recreated in either MHC-matched or MHC-mismatched contexts. However, donor and recipient tissue-resident immunity may continue to change over time. Post-transplant infections forming new immunological memory may lead to an increased TRL pool within the graft. The level of MHC mismatch and type of immunosuppression likely affects TRL maintenance and function but requires further investigation and could lead to better overall transplantation outcomes.

Limitations of study

Our models of nonarterialized liver and heterotopic heart transplantation do not fully recapitulate the human situation and present challenges when comparing to nontransplanted organs. Examination of the tissue-resident phenotype of donor and recipient cells is complicated by the potential recirculation of cells and the unknown time frame for acquisition of a tissue-resident phenotype after proliferation. Although graft-infiltrating recipient cells possessed a distinct phenotype, the significance of this for graft outcome and infection risk remains unclear. Finally, although *Rag1*$^{-/-}$ mice lack T and B cells, conventional immunosuppression suppresses only some aspects of the immune response and thus would have a less profound impact than complete removal of these cells. This is a descriptive study, and further work is needed to elucidate the functional role of TRLs in transplantation tolerance and post-transplant infection and cancer prevention.

STAR★METHODS

Detailed methods are provided in the online version of this paper and include the following:

- KEY RESOURCES TABLE
- RESOURCE AVAILABILITY
  - Lead contact
  - Materials availability
  - Data and code availability
- EXPERIMENTAL MODEL AND SUBJECT DETAILS
  - Animals
  - Orthotopic liver transplantation
  - Heterotopic heart transplantation
- METHOD DETAILS
  - Sample collection and isolation of tissue leukocytes
  - Flow cytometry analysis
  - *Ex vivo* leukocyte stimulation
  - Histology
  - Graphical abstract
- QUANTIFICATION AND STATISTICAL ANALYSIS

Figure 5. MHC-mismatched liver, but not heart, transplants survive after transient rejection despite depletion of donor lymphocytes and graft infiltration by cytotoxic recipient cells

(A) Survival of MHC-matched (n = 30) and MHC-mismatched (n = 14) liver transplants.

(B) Histology of MHC-matched and MHC-mismatched liver grafts at days 7 and 28. Scale bars indicate 200 μm (top panel) and 100 μm (bottom panel).

(C) Donor and recipient lymphocyte numbers after MHC-mismatched liver transplantation (n = 3–10).

(D) Recipient T cell expression of granzyme B, IFNγ, and IL-10 at day 7 (n = 3, 2-way ANOVA).

(E) Donor lymphocyte numbers at baseline (n = 3) and day 7 after MHC-mismatched transplantation to *Rag1*$^{-/-}$ recipients (n = 3, unpaired t test and Mann-Whitney test).

(F) Survival of syngeneic, MHC-matched congenic, and MHC-mismatched heart transplants (n = 5–7 per group).

(G) Donor and recipient lymphocyte numbers after MHC-mismatched heart transplantation (n = 3–5).

Data are means with SEM. Symbols indicate: *p < 0.05; **p < 0.01; ***p < 0.001; ****p < 0.0001. See also Figure S5.

SUPPLEMENTAL INFORMATION

Supplemental information can be found online at https://doi.org/10.1016/j.celrep.2021.109141.

ACKNOWLEDGMENTS

We thank the Centre for Microscopy, Characterisation & Analysis, funded by The University of Western Australia (UWA) and Western Australian State and Australian Commonwealth governments; UWA Animal Care Services; and Dr. B. Lu, H. Li, and Dr. A. McDonnell for their assistance. The MR1 tetramer was developed by Dr. James McCluskey, Dr. Jamie Rossjohn, and Dr. David Fairlie and produced by the NIH Tetramer Core Facility as permitted to be distributed by the University of Melbourne. The Western Australian Department of Health, the Charlies Foundation for Research, and the Sir Charles Gairdner Hospital and Osborne Park Health Care Group (RAC 2018-19/030) funded this work. A.P. was supported by an Australian Government Research Training Program Scholarship, and A.K. was supported by a National Health and Medical Research Council Senior Research Fellowship (1139607).

AUTHOR CONTRIBUTIONS

Conceptualization, A.P., L.D., A.K., and M.L.; data curation, A.P.; formal analysis, A.P. and S.D.; funding acquisition, A.P., G.P.J., L.D., and M.L.; investigation, A.P., W.H.H., L.L., S.D., M.W., B.d.B., and P.K.; methodology, A.P., W.H.H., L.L., and I.L.-C.; project administration, A.P. and M.L.; supervision, S.G., G.P.J., L.D., A.K., and M.L.; visualization, A.P. and S.D.; writing – original draft, A.P., A.L., A.K., and M.L.; writing – review & editing A.P., S.D., A.L., S.G., A.K., and M.L.

DECLARATION OF INTERESTS

The authors declare no competing interests.

Received: September 8, 2020
Revised: February 10, 2021
Accepted: April 26, 2021
Published: May 18, 2021

REFERENCES

Allie, S.R., Bradley, J.E., Mudunuru, U., Schultz, M.D., Graf, B.A., Lund, F.E., and Randall, T.D. (2019). The establishment of resident memory B cells in the lung requires local antigen encounter. Nat. Immunol. *20*, 97–108.

ANZCOTR (2018). 23rd Annual Report, 1984–2018 (The Australian and New Zealand Cardiothoracic Organ Transplant Registry).

ANZDATARegistry (2018). 41st Report, *Chapter 7* (Kidney Transplantation. Australia and New Zealand Dialysis and Transplant Registry).

ANZLITR (2020). 30th Annual Report on Liver and Intestinal Transplantation Activity to 31/12/2018 (Australia and New Zealand Liver and Intestinal Transplant Registry).

Ariotti, S., Hogenbirk, M.A., Dijkgraaf, F.E., Visser, L.L., Hoekstra, M.E., Song, J.Y., Jacobs, H., Haanen, J.B., and Schumacher, T.N. (2014). T cell memory. Skin-resident memory $CD8^+$ T cells trigger a state of tissue-wide pathogen alert. Science *346*, 101–105.

Belz, G.T., Denman, R., Seillet, C., and Jacquelot, N. (2020). Tissue-resident lymphocytes: weaponized sentinels at barrier surfaces. F1000Res. *9*, F1000 Faculty Rev-691.

Beura, L.K., Fares-Frederickson, N.J., Steinert, E.M., Scott, M.C., Thompson, E.A., Fraser, K.A., Schenkel, J.M., Vezys, V., and Masopust, D. (2019). $CD4^+$ resident memory T cells dominate immunosurveillance and orchestrate local recall responses. J. Exp. Med. *216*, 1214–1229.

Cheroutre, H., and Lambolez, F. (2008). Doubting the TCR coreceptor function of CD8alphaalpha. Immunity *28*, 149–159.

Corry, R.J., Winn, H.J., and Russell, P.S. (1973). Heart transplantation in congenic strains of mice. Transplant. Proc. *5*, 733–735.

de Leur, K., Dieterich, M., Hesselink, D.A., Corneth, O.B.J., Dor, F.J.M.F., de Graav, G.N., Peeters, A.M.A., Mulder, A., Kimenai, H.J.A.N., Claas, F.H.J., et al. (2019). Characterization of donor and recipient CD8+ tissue-resident memory T cells in transplant nephrectomies. Sci. Rep. *9*, 5984.

Elkins, W.L., and Guttmann, R.D. (1968). Pathogenesis of a local graft versus host reaction: immunogenicity of circulating host leukocytes. Science *159*, 1250–1251.

Fan, X., and Rudensky, A.Y. (2016). Hallmarks of Tissue-Resident Lymphocytes. Cell *164*, 1198–1211.

Feng, S., and Bucuvalas, J. (2017). Tolerance after liver transplantation: Where are we? Liver Transpl. *23*, 1601–1614.

Fernandez-Ruiz, D., Ng, W.Y., Holz, L.E., Ma, J.Z., Zaid, A., Wong, Y.C., Lau, L.S., Mollard, V., Cozijnsen, A., Collins, N., et al. (2016). Liver-Resident Memory $CD8^+$ T Cells Form a Front-Line Defense against Malaria Liver-Stage Infection. Immunity *45*, 889–902.

Feuerer, M., Herrero, L., Cipolletta, D., Naaz, A., Wong, J., Nayer, A., Lee, J., Goldfine, A.B., Benoist, C., Shoelson, S., and Mathis, D. (2009). Lean, but not obese, fat is enriched for a unique population of regulatory T cells that affect metabolic parameters. Nat. Med. *15*, 930–939.

Gasteiger, G., Fan, X., Dikiy, S., Lee, S.Y., and Rudensky, A.Y. (2015). Tissue residency of innate lymphoid cells in lymphoid and nonlymphoid organs. Science *350*, 981–985.

Gebhardt, T., Palendira, U., Tscharke, D.C., and Bedoui, S. (2018). Tissue-resident memory T cells in tissue homeostasis, persistent infection, and cancer surveillance. Immunol. Rev. *283*, 54–76.

Geissmann, F., Cameron, T.O., Sidobre, S., Manlongat, N., Kronenberg, M., Briskin, M.J., Dustin, M.L., and Littman, D.R. (2005). Intravascular immune surveillance by CXCR6+ NKT cells patrolling liver sinusoids. PLoS Biol. *3*, e113.

Gill, U.S., Pallett, L.J., Thomas, N., Burton, A.R., Patel, A.A., Yona, S., Kennedy, P.T.F., and Maini, M.K. (2019). Fine needle aspirates comprehensively sample intrahepatic immunity. Gut *68*, 1493–1503.

Haddadi, S., Thanthrige-Don, N., Afkhami, S., Khera, A., Jeyanathan, M., and Xing, Z. (2017). Expression and role of VLA-1 in resident memory CD8 T cell responses to respiratory mucosal viral-vectored immunization against tuberculosis. Sci. Rep. *7*, 9525.

Heesch, K., Raczkowski, F., Schumacher, V., Hünemörder, S., Panzer, U., and Mittrücker, H.W. (2014). The function of the chemokine receptor CXCR6 in the T cell response of mice against Listeria monocytogenes. PLoS ONE *9*, e97701.

Holz, L.E., Prier, J.E., Freestone, D., Steiner, T.M., English, K., Johnson, D.N., Mollard, V., Cozijnsen, A., Davey, G.M., Godfrey, D.I., et al. (2018). $CD8^+$ T Cell Activation Leads to Constitutive Formation of Liver Tissue-Resident Memory T Cells that Seed a Large and Flexible Niche in the Liver. Cell Rep. *25*, 68–79.e4.

Hossain, M.S., Takimoto, H., Ninomiya, T., Yoshida, H., Kishihara, K., Matsuzaki, G., Kimura, G., and Nomoto, K. (2000). Characterization of CD4− CD8− CD3+ T-cell receptor-alphabeta+ T cells in murine cytomegalovirus infection. Immunology *101*, 19–29.

Johnson, J.L., Rosenthal, R.L., Knox, J.J., Myles, A., Naradikian, M.S., Madej, J., Kostiv, M., Rosenfeld, A.M., Meng, W., Christensen, S.R., et al. (2020). The Transcription Factor T-bet Resolves Memory B Cell Subsets with Distinct Tissue Distributions and Antibody Specificities in Mice and Humans. Immunity *52*, 842–855.e6.

Klose, C.S., and Artis, D. (2016). Innate lymphoid cells as regulators of immunity, inflammation and tissue homeostasis. Nat. Immunol. *17*, 765–774.

Li, F., Hao, X., Chen, Y., Bai, L., Gao, X., Lian, Z., Wei, H., Sun, R., and Tian, Z. (2017). The microbiota maintain homeostasis of liver-resident $\gamma\delta$T-17 cells in a lipid antigen/CD1d-dependent manner. Nat. Commun. *7*, 13839.

Mackay, L.K., and Kallies, A. (2017). Transcriptional Regulation of Tissue-Resident Lymphocytes. Trends Immunol. *38*, 94–103.

Mackay, L.K., Wynne-Jones, E., Freestone, D., Pellicci, D.G., Mielke, L.A., Newman, D.M., Braun, A., Masson, F., Kallies, A., Belz, G.T., and Carbone, F.R. (2015). T-box Transcription Factors Combine with the Cytokines TGF-β

and IL-15 to Control Tissue-Resident Memory T Cell Fate. Immunity *43*, 1101–1111.

Mackay, L.K., Minnich, M., Kragten, N.A., Liao, Y., Nota, B., Seillet, C., Zaid, A., Man, K., Preston, S., Freestone, D., et al. (2016). Hobit and Blimp1 instruct a universal transcriptional program of tissue residency in lymphocytes. Science *352*, 459–463.

Makita, S., Kanai, T., Nemoto, Y., Totsuka, T., Okamoto, R., Tsuchiya, K., Yamamoto, M., Kiyono, H., and Watanabe, M. (2007). Intestinal lamina propria retaining CD4+CD25+ regulatory T cells is a suppressive site of intestinal inflammation. J. Immunol. *178*, 4937–4946.

Milner, J.J., Toma, C., He, Z., Kurd, N.S., Nguyen, Q.P., McDonald, B., Quezada, L., Widjaja, C.E., Witherden, D.A., Crowl, J.T., et al. (2020). Heterogenous Populations of Tissue-Resident CD8$^+$ T Cells Are Generated in Response to Infection and Malignancy. Immunity *52*, 808–824.e7.

Monaco, G., Chen, H., Poidinger, M., Chen, J., de Magalhães, J.P., and Larbi, A. (2016). flowAI: automatic and interactive anomaly discerning tools for flow cytometry data. Bioinformatics *32*, 2473–2480.

Norris, S., Collins, C., Doherty, D.G., Smith, F., McEntee, G., Traynor, O., Nolan, N., Hegarty, J., and O'Farrelly, C. (1998). Resident human hepatic lymphocytes are phenotypically different from circulating lymphocytes. J. Hepatol. *28*, 84–90.

OPTN/SRTR (2020). 2018 Annual Report of the U.S. Organ Procurement and Transplantation Network and the Scientific Registry of Transplant Recipients: Transplant Data 2007–2018. Department of Health and Human Services, Health Resources and Services Administration, Healthcare Systems Bureau, Division of Transplantation; United Network for Organ Sharing (University Renal Research and Education Association).

Pallett, L.J., Davies, J., Colbeck, E.J., Robertson, F., Hansi, N., Easom, N.J.W., Burton, A.R., Stegmann, K.A., Schurich, A., Swadling, L., et al. (2017). IL-2^{high} tissue-resident T cells in the human liver: Sentinels for hepatotropic infection. J. Exp. Med. *214*, 1567–1580.

Pallett, L.J., Burton, A.R., Amin, O.E., Rodriguez-Tajes, S., Patel, A.A., Zakeri, N., Jeffery-Smith, A., Swadling, L., Schmidt, N.M., Baiges, A., et al. (2020). Longevity and replenishment of human liver-resident memory T cells and mononuclear phagocytes. J. Exp. Med. *217*, e20200050.

Poussier, P., Ning, T., Banerjee, D., and Julius, M. (2002). A unique subset of self-specific intraintestinal T cells maintains gut integrity. J. Exp. Med. *195*, 1491–1497.

Prosser, A.C., Kallies, A., and Lucas, M. (2018). Tissue-Resident Lymphocytes in Solid Organ Transplantation: Innocent Passengers or the Key to Organ Transplant Survival? Transplantation *102*, 378–386.

Qian, S., Demetris, A.J., Murase, N., Rao, A.S., Fung, J.J., and Starzl, T.E. (1994). Murine liver allograft transplantation: tolerance and donor cell chimerism. Hepatology *19*, 916–924.

Salou, M., Legoux, F., Gilet, J., Darbois, A., du Halgouet, A., Alonso, R., Richer, W., Goubet, A.G., Daviaud, C., Menger, L., et al. (2019). A common transcriptomic program acquired in the thymus defines tissue residency of MAIT and NKT subsets. J. Exp. Med. *216*, 133–151.

Sen, A., Callisen, H., Libricz, S., and Patel, B. (2019). Complications of Solid Organ Transplantation: Cardiovascular, Neurologic, Renal, and Gastrointestinal. Crit. Care Clin. *35*, 169–186.

Snyder, M.E., Finlayson, M.O., Connors, T.J., Dogra, P., Senda, T., Bush, E., Carpenter, D., Marboe, C., Benvenuto, L., Shah, L., et al. (2019). Generation and persistence of human tissue-resident memory T cells in lung transplantation. Sci. Immunol. *4*, eaav5581.

Steinert, E.M., Schenkel, J.M., Fraser, K.A., Beura, L.K., Manlove, L.S., Igyártó, B.Z., Southern, P.J., and Masopust, D. (2015). Quantifying Memory CD8 T Cells Reveals Regionalization of Immunosurveillance. Cell *161*, 737–749.

Taner, T. (2017). Liver transplantation: Rejection and tolerance. Liver Transpl. *23* (*S1*), S85–S88.

Tay, S.S., Lu, B., Sierro, F., Benseler, V., McGuffog, C.M., Bishop, G.A., Cowan, P.J., McCaughan, G.W., Dwyer, K.M., Bowen, D.G., and Bertolino, P. (2013). Differential migration of passenger leukocytes and rapid deletion of naive alloreactive CD8 T cells after mouse liver transplantation. Liver Transpl. *19*, 1224–1235.

Topham, D.J., and Reilly, E.C. (2018). Tissue-Resident Memory CD8$^+$ T Cells: From Phenotype to Function. Front. Immunol. *9*, 515.

Vinton, C.L., Ortiz, A.M., Calantone, N., Mudd, J.C., Deleage, C., Morcock, D.R., Whitted, S., Estes, J.D., Hirsch, V.M., and Brenchley, J.M. (2017). Cytotoxic T Cell Functions Accumulate When CD4 Is Downregulated by CD4$^+$ T Cells in African Green Monkeys. J. Immunol. *198*, 4403–4412.

Walsh, D.A., Borges da Silva, H., Beura, L.K., Peng, C., Hamilton, S.E., Masopust, D., and Jameson, S.C. (2019). The Functional Requirement for CD69 in Establishment of Resident Memory CD8$^+$ T Cells Varies with Tissue Location. J. Immunol. *203*, 946–955.

Yokota, S., Ueki, S., Ono, Y., Kasahara, N., Pérez-Gutiérrez, A., Kimura, S., Yoshida, O., Murase, N., Yasuda, Y., Geller, D.A., and Thomson, A.W. (2016). Orthotopic mouse liver transplantation to study liver biology and allograft tolerance. Nat. Protoc. *11*, 1163–1174.

Zhai, Y., Shen, X.D., Gao, F., Zhao, A., Freitas, M.C., Lassman, C., Luster, A.D., Busuttil, R.W., and Kupiec-Weglinski, J.W. (2008). CXCL10 regulates liver innate immune response against ischemia and reperfusion injury. Hepatology *47*, 207–214.

STAR★METHODS

KEY RESOURCES TABLE

REAGENT or RESOURCE	SOURCE	IDENTIFIER
Antibodies		
CD117 (c-Kit) Brilliant UV 395 (2B8)	BD Biosciences	Cat#564011 RRID:AB_2738541
CD11c AlexaFluor 700 (N418)	Thermo Fisher	Cat#56-0114-82 RRID:AB_493992
CD127 PE (A7R34)	BioLegend	Cat#135009 RRID:AB_1937252
CD127 PE/CF594 (SB/199)	BD Biosciences	Cat#562419 RRID:AB_11153131
CD19 Brilliant Violet 480 (1D3)	BD Biosciences	Cat#566107 RRID:AB_2739509
CD19 Brilliant Violet 510 (1D3)	BD Biosciences	Cat#562956 RRID:AB_2737915
CD25 Brilliant Violet 786 (PC61)	BD Biosciences	Cat#564023 RRID:AB_2738548
CD3 Brilliant Violet 510 (145-2C11)	BD Biosciences	Cat#563024 RRID:AB_2737959
CD3 PerCP/eF710 (17A2)	Thermo Fisher	Cat#46-0032-82 RRID:AB_1834427
CD4 AlexaFluor 700 (RM4-5)	BD Biosciences	Cat#561025 RRID:AB_2034006
CD4 Brilliant Violet 786 (GK1.5)	BD Biosciences	Cat#563331 RRID:AB_2738140
CD44 Brilliant Blue 515 (IM7)	BD Biosciences	Cat#564587 RRID:AB_2738855
CD44 Brilliant Violet 510 (IM7)	BD Biosciences	Cat#563114 RRID:AB_2738011
CD45.1 APC/eFluor 780 (A20)	Thermo Fisher	Cat#47-0453-82 RRID:AB_1582228
CD45.1 Brilliant Violet 711 (A20)	BD Biosciences	Cat#563982 RRID:AB_2861197
CD45.2 AlexaFluor 700 (104)	BD Biosciences	Cat#560693 RRID:AB_1727491
CD45.2 APC/eFluor 780 (104)	Thermo Fisher	Cat#47-0454-82 RRID:AB_1272175
CD45.2 FITC (104)	BD Biosciences	Cat#561874 RRID:AB_10894189
CD45.2 PerCP/Cy5.5 (104)	BD Biosciences	Cat#561096 RRID:AB_2034008
CD49a Brilliant Blue 700 (Ha31/8)	BD Biosciences	Cat#742164 RRID:AB_2861198
CD49a Brilliant UV 395 (Ha31/8)	BD Biosciences	Cat#740262 RRID:AB_2740005
CD49a Brilliant Violet 510 (Ha31/8)	BD Biosciences	Cat#740144 RRID:AB_2739900
CD49a PE (Ha31/8)	BD Biosciences	Cat#562115 RRID:AB_11153117
CD49b PE/Cy7 (DX5)	BioLegend	Cat#108922 RRID:AB_2561460
CD49d Brilliant Violet 711 (R1-2)	BD Biosciences	Cat#740661 RRID:AB_2740350
CD62L eVolve 605 (MEL-14)	Thermo Fisher	Cat#83-0621-42 RRID:AB_2574718
CD62L PE/Cy7 (MEL-14)	BD Biosciences	Cat#560516 RRID:AB_1645257
CD69 Brilliant Violet 711 (H1.2F3)	BD Biosciences	Cat#740664 RRID:AB_2740352
CD69 PE/Cy7 (H1.2F3)	BD Biosciences	Cat#552879 RRID:AB_394508
CD69 PE/Dazzle 594 (H1.2F3)	BioLegend	Cat#104536 RRID:AB_2565583
CD8α Brilliant UV 395 (53-6.7)	BD Biosciences	Cat#563786 RRID:AB_2732919
CD8α eVolve 655 (53-6.7)	Thermo Fisher	Cat#86-0081-42 RRID:AB_2574784
CD8α SuperBright 645 (53-6.7)	Thermo Fisher	Cat#64-0081-82 RRID:AB_2662353
CD8β Brilliant UV 395 (H35-17.2)	BD Biosciences	Cat#740278 RRID:AB_2740017
CD8β Brilliant Violet 480 (H35-17.2)	BD Biosciences	Cat#746835 RRID:AB_2744086
CX3CR1 Brilliant Violet 421 (SA011F11)	BioLegend	Cat#149023 RRID:AB_2565706
CXCR3 Brilliant Violet 650 (CXCR3-173)	BioLegend	Cat#126531 RRID:AB_2563160
CXCR6 PE (SA051D1)	BioLegend	Cat#151103 RRID:AB_2566545
Eomes PE/Cy7 (Dan11mag)	Thermo Fisher	Cat#25-4875-80 RRID:AB_2573453
FoxP3 AlexaFluor 647 (150D)	BioLegend	Cat#320014 RRID:AB_439750
FoxP3 PE/CF594 (MF223)	BD Biosciences	Cat#562466 RRID:AB_11151905
GATA-3 Brilliant Violet 421 (L50-823)	BD Biosciences	Cat#563349 RRID:AB_2738152
IFNγ Brilliant Violet 785 (XMG1.2)	BioLegend	Cat#505837 RRID:AB_11219004

(*Continued on next page*)

Continued

REAGENT or RESOURCE	SOURCE	IDENTIFIER
IL-10 Brilliant Violet 421 (JES5-16E3)	BD Biosciences	Cat#563276 RRID:AB_2738111
Ki67 Brilliant Violet 786 (B5)	BD Biosciences	Cat#563756 RRID:AB_2732007
Ki67 PerCP/eFluor 710 (SolA15)	Thermo Fisher	Cat#46-5698-80 RRID:AB_11039489
KLRG1 Brilliant Violet 711 (2F1)	BD Biosciences	Cat#564014 RRID:AB_2738542
LAG-3 Brilliant Violet 650 (C9B7W)	BioLegend	Cat#125227 RRID:AB_2687209
Lin PerCP/Cy5.5 ()	BD Biosciences	Cat#561317 RRID:AB_10612020
Ly6C PE/Cy7 (AL-21)	BD Biosciences	Cat#560593 RRID:AB_1727557
NK1.1 APC (PK136)	BD Biosciences	Cat#550627 RRID:AB_398463
NKp46 AlexaFluor 647 (29A1.4)	BD Biosciences	Cat#560755 RRID:AB_1727464
PD-1 Brilliant Violet 421 (J43)	BD Biosciences	Cat#565942 RRID:AB_2739406
RORγt Brilliant Violet 650 (Q31-378)	BD Biosciences	Cat#564722 RRID:AB_2738915
ST2 PE (RMST2-2)	Thermo Fisher	Cat#12-9335-82 RRID:AB_2572708
Tbet Brilliant Violet 421 (O4-46)	BD Biosciences	Cat#563318 RRID:AB_2687543
Tbet Brilliant Violet 605 (4B10)	BioLegend	Cat#644817 RRID:AB_11219388
TCRβ AlexaFluor 700 (H57-597)	BioLegend	Cat#109223 RRID:AB_1027654
TCRβ Brilliant Violet 421 (H57-597)	BioLegend	Cat#109229 RRID:AB_10933263
TCRγδ Brilliant Violet 711 (GL3)	BD Biosciences	Cat#563994 RRID:AB_2738531
TCRγδ PE (GL3)	BD Biosciences	Cat#561997 RRID:AB_10897008
TIM-3 PE (5D12)	BD Biosciences	Cat#566346 RRID:AB_2739702
Chemicals, peptides, and recombinant proteins		
CD1d tetramer APC (αGalCer loaded)	ProImmune	Cat#E001-4A-G
CD1d tetramer PE (αGalCer loaded)	ProImmune	Cat#E001-2B-E
MR1 tetramer Brilliant Violet 421 (5-OP-RU)	NIH	N/A
DNase I	Thermo Fisher	AM2224
PBS tablets	Thermo Fisher	18912014
Newborn calf serum (heat-inactivated)	Thermo Fisher	26010-074
DMEM	Thermo Fisher	10569010
Red Blood Cell Lysis Solution	Miltenyi Biotec	130-094-183
Percoll	Cytiva Life Sciences	17-0891-01
Collagenase II	Worthington Biochemicals	CLS-2
Critical commercial assays		
FoxP3/Transcription Factor Staining Buffer Set	Thermo Fisher	Cat#00-5523-00
Zombie UV Fixable Viability Kit	BioLegend	Cat#423107
Cell Activation Cocktail (with Brefeldin A)	BioLegend	423304
Stabilizing Fixative	BD Biosciences	Cat#338036
Brilliant Stain Buffer	BD Biosciences	Cat# 566349
Experimental models: Organisms/strains		
CD45.1 (B6.SJL-Ptprc^{a}Pepc^{b}/BoyJArc)	Animal Resources Centre	PTP
CD45.1 (B6.SJL-Ptprc^{a}Pepc^{b}/BoyJAusb)	Australian Bioresources	N/A
CD45.2 (C57BL/6J)	Animal Resources Centre	B6
RAG1$^{-/-}$ (B6.SVJ129-Rag1tm1Bal/Arc)	Animal Resources Centre	RAG1 N10
Software and algorithms		
FlowJo v10	Treestar Inc	RRID: SCR_008520
Prism 8	Graphpad Inc	RRID: SCR_002798
Other		
UltraComp eBeads Compensation Beads	Thermo Fisher	Cat#01-2222-42
Ultra Rainbow Calibration Kit	Spherotec	Cat#URCP-38-2K
Cytometer Setup and Tracking Beads	BD Biosciences	Cat#655051

RESOURCE AVAILABILITY

Lead contact

Further information and requests for resources and reagents should be directed to and will be fulfilled by the lead contact, Michaela Lucas (michaela.lucas@uwa.edu.au).

Materials availability

This study did not generate new unique reagents.

Data and code availability

This study did not generate datasets or code.

EXPERIMENTAL MODEL AND SUBJECT DETAILS

Animals

CD45.2 C57BL/6J and BALB/c, CD45.1 C57BL/6 (B6.SJL-Ptprc^{a}Pepc^{b}/BoyJ), CD45.1 BALB/c (CByJ.SJL(B6)-Ptprc^{a}/J), and *Rag1*$^{-/-}$ (B6.SVJ129-Rag1tm1Bal/Arc) mice were purchased from the Animal Resources Centre or Australian Bioresources. All strains except *Rag1*$^{-/-}$ are immunocompetent and were housed under standard specific pathogen-free conditions. *Rag1*$^{-/-}$ mice are mutant inbred homozygotes for the *Rag1*^{tm1Bal} mutation and produce no mature T or B cells. These mice are considered severely immunocompromised and thus were housed in individually ventilated cages. Prior to transplantation, all mice were drug and test naive and had not undergone any previous procedures. All mice were monitored daily, housed at a maximum of 6 mice per cage, and fed normal chow. All animal experiments were conducted with approval of the University of Western Australia Animal Ethics Committee under protocol numbers RA/3/100/1364 and RA/3/100/1568 and conformed to the Australian Code for the Care and Use of Animals for Scientific Purposes.

Orthotopic liver transplantation

MHC matched transplantation was performed with randomly selected, weight matched adult male CD45.1 C57BL/6 H2k^{b} donor mice and male CD45.2 C57BL/6J H2k^{b} recipient mice, each weighing 25-30 g (approximately 12 weeks of age). Males were used for their larger size compared to females to provide maximal vasculature and bile duct size. MHC mismatched transplantation was performed with CD45.1 C57BL/6 H2k^{b} donor mice and male CD45.2 BALB/c H2k^{d} recipient mice. *Rag1*$^{-/-}$ transplants were performed with CD45.1 C57BL/6 or CD45.1 BALB/c donor mice. A pre-operative dose of 0.05-0.1 mg/kg buprenorphine was administered subcutaneously to all transplant recipient mice and general anesthetic induced by continuous isoflurane inhalation. Non-arterialized orthotopic liver transplantation was performed as previously described (Yokota et al., 2016). Mice were individually housed during post-surgical recovery. Cages were placed on a heated mat under heat lamp for immediate post-transplant monitoring every 15 min for the first hour, then every 30 min to a total of 3 h. Mice were placed in a warming cabinet at 26°C for the first 7 post-surgical days. Mice were monitored twice daily for the first 3 post-surgical days and administered buprenorphine (0.05-0.1 mg/kg) subcutaneously for analgesia twice daily as required. Monitoring was reduced to once per day to day 7 post-transplant, then twice per week to day 28 post-transplant. No immunosuppressive therapies were administered before or after transplantation.

Heterotopic heart transplantation

Randomly selected female CD45.1 C57BL/6 mice were used as donors and female CD45.2 C57BL/6J or BALB/c mice as recipients for heart transplantation at 6-8 weeks of age. Females were selected due to their increased abdominal space compared to male mice. A pre-operative dose of 0.05-0.1 mg/kg buprenorphine was administered subcutaneously to all transplant recipient mice and general anesthetic induced by continuous isoflurane inhalation. Intra-abdominal vascularised heart transplantation was performed as described previously (Corry et al., 1973). Post-operative housing and analgesia was performed as per the liver transplant protocol above.

METHOD DETAILS

Sample collection and isolation of tissue leukocytes

At designated post-operative time points the transplanted liver or heart, spleen, abdominal lymph nodes, peripheral blood (half clotted for serum, half collected into heparinised tubes for flow cytometry) and hind limb bone marrow were harvested from each transplant recipient. The native heart was also collected from heart transplant recipient mice. The liver was perfused with 10 mL and hearts with 5 mL cold saline prior to collection. Hearts were cut longitudinally and injected with 500 μL of DMEM containing 400 U/mL collagenase II (Worthington Biochemicals) and 48 U/mL DNase I (Thermo Fisher). Heart sections were incubated in 5 mL of this digestion cocktail for 10 min at 37°C with gentle shaking before being minced and incubated in the same conditions for a further 30 min. All organs were passed through 70 μm cell strainers. Leukocytes were isolated from liver and heart single cell suspensions by 42% Percoll density-gradient centrifugation. Red cells were lysed from all tissue samples with 1x Red Blood Cell Lysis Buffer (Miltenyi Biotec), as recommended by the manufacturer. Cells were counted on a Countess II FL Automated Cell Counter (Thermo Fisher).

Flow cytometry analysis

Leukocytes (0.1-4 × 10^6) were stained with antibodies and tetramers listed in the Key resources table. Intracellular staining was performed with Foxp3/Transcription Factor Staining Buffer Set (Thermo Fisher) as per the manufacturer's instructions. Viability was determined using Zombie UV™ Fixable Viability Dye (BioLegend). Proliferation was assessed by intracellular Ki67 staining. Antibodies and tetramers were titrated for optimal population resolution. Fluorescence minus one controls were completed for all panels to determine gating limits and fluorescence spread. Data was acquired on a BD SORP Fortessa™ flow cytometer with daily quality control checks performed with Cytometer Setup and Tracking beads (BD Biosciences) and Ultra Rainbow Calibration Particles (Spherotech). Data was analyzed using Flowjo software (BD). All samples were subject to FlowAI (Monaco et al., 2016) prior to further analysis for removal of anomalous data points. All blood data presented is per mL of blood. Lymphocyte subset gating strategies are shown in Figures S1A and S1B. Baseline organs analyzed were from mice age- and sex-matched to relevant transplant organ donors.

Ex vivo leukocyte stimulation

Between 1 and 4 × 10^6 cells per well in a 96-well plate were incubated in 200 μL of Dulbecco's Modified Eagle Medium (Thermo Fisher) with 10% (v/v) newborn calf serum (Thermo Fisher) with or without Cell Activation Cocktail (PMA/Ionomycin) containing Brefeldin A (BioLegend) diluted 500x as per the manufacturer's instructions. Cells were incubated at 37°C for 4 h with 5% CO_2. Stimulation was halted by washing with PBS and cells were stained for flow cytometry as above.

Histology

A section of the left lateral lobe of each transplanted liver was taken for histology. Tissue was fixed in 10% phosphate-buffered formalin and embedded in paraffin. Staining with hematoxylin and eosin was performed at PathWest Laboratory Medicine WA and assessed for evidence of rejection by an experienced histopathologist.

Graphical abstract

The image was created with BioRender.com.

QUANTIFICATION AND STATISTICAL ANALYSIS

All statistical analysis was performed in GraphPad Prism 8. Data was tested for outliers and normal distribution prior to statistical testing and analysis. Tests used and n values for number of baseline mice or transplants are included in individual figure legends. All data shown is mean with SEM. Sidak's correction for multiple comparisons was used where appropriate. Standard symbols indicate: *$p < 0.05$, **$p < 0.01$, ***$p < 0.001$, ****$p < 0.0001$.